

# Detecting Stars at the Galactic Centre via Synchrotron Emission

Idan Ginsburg<sup>\*</sup>, Xiawei Wang<sup>†</sup>, Abraham Loeb<sup>‡</sup> & Ofer Cohen<sup>§</sup>

*Astronomy Department, Harvard University, 60 Garden St., Cambridge, MA 02138, USA*

9 March 2022

## ABSTRACT

Stars orbiting within  $1''$  of the supermassive black hole in the Galactic Centre, Sgr A<sup>\*</sup>, are notoriously difficult to detect due to obscuration by gas and dust. We show that some stars orbiting this region may be detectable via synchrotron emission. In such instances, a bow shock forms around the star and accelerates the electrons. We calculate that around the 10 GHz band (radio) and at  $10^{14}$  Hz (infrared) the luminosity of a star orbiting the black hole is comparable to the luminosity of Sgr A<sup>\*</sup>. The strength of the synchrotron emission depends on a number of factors including the star’s orbital velocity. Thus, the ideal time to observe the synchrotron flux is when the star is at pericenter. The star S2 will be  $\sim 0.015''$  from Sgr A<sup>\*</sup> in 2018, and is an excellent target to test our predictions.

**Key words:** general-black hole physics-Galaxy:centre-Galaxy:kinematics and dynamics-stellar dynamics

## 1 INTRODUCTION

Over 100 young massive stars inhabit the central parsec of the Milky Way (for a review see Genzel et al. 2010; Mapelli & Gualandris 2015). The stars whose orbit lies within  $\sim 0.04$  pc from the Galactic Centre (GC) are known as the S-stars (e.g. Schödel et al. 2003; Ghez et al. 2005). The orbits of 28 S-stars were determined by Gillessen et al. (2009). 19 members have semimajor axis  $a \leq 1$  arcsec. Of those, 16 are B stars and the rest late-type stars. Of particular interest is the star S2 (also known as SO-2) which has been observed for more than one complete orbit (Ghez et al. 2005; Ghez et al. 2008; Gillessen et al. 2009). S2 orbits the supermassive black hole, Sgr A<sup>\*</sup>, every 15.9 years. It is a B0-2.5 V main sequence star with an estimated mass of  $\sim 15M_{\odot}$  (Martins et al. 2008). The second complete orbit of a star around Sgr A<sup>\*</sup> was announced not long ago (Meyer et al. 2012). This star, S102 (also known as SO-102) has a period of 11.5 years and is about 16 times fainter than S2. Both S2 and S102 provide compelling evidence that Sgr A<sup>\*</sup> has a mass of  $\sim 4 \times 10^6 M_{\odot}$ .

The detection of young, massive stars with orbits close to Sgr A<sup>\*</sup> was surprising (eg. Ghez et al. 2003). A number of possible mechanisms have been proposed to account

for the origin of the S-stars. Löckmann et al. (2008) argued that the dynamical interaction of two stellar disks in the central parsec could lead to the formation of the S-stars. Griv (2010) proposed that the S-stars were born in the disk and migrated inward. Recently, Chen & Amaro-Seoane (2014) theorized that a few Myr ago the disk extended down to the innermost region around Sgr A<sup>\*</sup> and Kozai-Lidov-like resonance resulted in the S-stars. Perhaps the simplest and arguably most likely scenario is that at least some of the S-stars are the result of a three-body interaction with Sgr A<sup>\*</sup> (e.g. Ginsburg & Loeb 2006; Ginsburg & Loeb 2007; Ginsburg et al. 2012; Zhang et al. 2013). In this scenario, a binary star system interacts with Sgr A<sup>\*</sup>, and tidal disruption leads to one star falling into the gravitational well of the black hole while the companion is ejected as a hypervelocity star (HVS) (Hills 1988). HVSs were first observed in 2005 (Brown et al. 2005) and as of today some 24 have been identified (see Brown et al. 2014 for the list). Brown et al. (2015) studied 12 confirmed HVSs and found that the vast majority are consistent with having a GC origin. Furthermore, observations indicate that these HVSs are likely massive slowly pulsating B stars (Ginsburg et al. 2013) and thus consistent with the known S-stars.

There are various candidate HVSs which are far less massive than B-type stars (Palladino et al. 2014; Zhong et al. 2014; Zhang et al. 2015). Given the fact that the stellar density in the central parsec is  $\sim 10^6 M_{\odot} \text{pc}^{-3}$  (Schödel et al. 2009) a distribution of masses is

<sup>\*</sup> E-mail: iginsburg@cfa.harvard.edu

<sup>†</sup> E-mail: xiawei.wang@cfa.harvard.edu

<sup>‡</sup> E-mail: aloeb@cfa.harvard.edu

<sup>§</sup> E-mail: ocohen@cfa.harvard.edu

expected. However, detecting stars at the GC is notoriously difficult due to dust extinction (e.g. Schödel et al. 2010). In this paper we discuss using synchrotron radio emission to observe and possibly monitor stars at the GC. Of particular importance is the fact that S2 will reach periape in 2017. We show that the closer S2 is to Sgr A\* the more likely we are detect the synchrotron emission. Thus, S2 serves as an ideal test subject. In Section 2 we provide the physics behind the synchrotron emission. In Section 3 we show that a star such as S2 may be observable via its synchrotron emission. We conclude with some discussions and future observations in Section 4.

## 2 SHOCKS AND SYNCHROTRON EMISSION

We consider stars orbiting Sgr A\*. Interactions between winds from such a star and the interstellar medium (ISM) will create two shocks, a reverse and forward shock. The forward shock propagates into the ambient medium which is swept up and subsequently compressed and accelerated. The faster wind is compressed and decelerated by the reverse shock. We are interested in the emission from electrons accelerated by the forward shock. In our case the forward shock is a bow shock with Mach angle  $\theta \sim \mathcal{M}^{-1}$ , where  $\mathcal{M}$  is the Mach number. In such a scenario, roughly half the star's mass loss contributes to the shock. The mechanical luminosity is simply given by kinetic energy which depends upon the mass loss rate,  $\dot{M}$ , and wind speed

$$L_w = \frac{1}{2} \dot{M}_w v_w^2. \quad (1)$$

For a massive star such as S2, typical values for  $\dot{M}_w$  are  $\sim 10^{-6} M_\odot \text{ yr}^{-1}$ ,  $v_w \sim 1000 \text{ km s}^{-1}$  and thus  $L_w$  is around  $10^{35} \text{ erg s}^{-1}$ . Consequently, the total non-thermal luminosity,  $L_{nt}$ , is given by the fraction of electrons,  $\epsilon_{nt}$ , accelerated to produce non-thermal radiation

$$L_{nt} = \epsilon_{nt} L_w. \quad (2)$$

We let  $\epsilon_{nt}$  be 5% although simulations show that this value is uncertain (Guo et al. 2014). The energy density of the amplified magnetic field is given by  $U_B = B^2/8\pi$ . Therefore, assuming equipartition of energy,  $U_B = \xi_B n_s k T_s$  leads to

$$B = (8\pi \xi_B n_s k T_s)^{1/2} \quad (3)$$

where  $\xi_B$  is the fraction of thermal energy in the magnetic field,  $n_s$  is the post-shock number density, and  $k T_s$  the temperature of the post-shock medium. In the strong shock limit for an adiabatic index of 5/3, the post-shock number density  $n_s$  is  $\sim 4$  times the number density of the ambient ISM. Although the value of  $\xi_B$  is highly uncertain, a value of 0.1 is reasonable (Völk et al. 2005). The resulting values for  $B$  are  $\sim 10^{-2} - 10^{-3} \text{ G}$ . The Rankine-Hugoniot jump conditions give the post shock temperature

$$T_s = \frac{[(\gamma_t - 1)\mathcal{M}^2 + 2][2\gamma_t\mathcal{M}^2 - (\gamma_t - 1)]}{(\gamma_t + 1)^2\mathcal{M}^2} T_o \quad (4)$$

where  $T_o$  is the upstream temperature, and  $\gamma_t$  is the adiabatic index which is taken to be 5/3. At the contact discontinuity, ram pressure from the star/ISM is balanced by ram pressure from the wind. Thus we have  $\rho_* v_*^2 = \rho_w v_w^2$  where

the mass flux is given as  $\rho_w v_w = \frac{\dot{M}_w}{4\pi R^2}$  and this leads to the standoff radius

$$R_o = \left( \frac{\dot{M}_w v_w}{4\pi \rho_* v_*^2} \right)^{1/2}. \quad (5)$$

$\rho_* = n_o m_p$  where  $m_p$  is the proton mass. At a distance of around 0.3 pc from Sgr A\*  $n_o \sim 10^3 \text{ cm}^{-3}$  and the temperature of the ISM is  $\sim 10^7 \text{ K}$  (Quataert 2004). Assuming  $v_* = 1000 \text{ km s}^{-1}$  a typical standoff radius is approximately  $10^{-3} \text{ pc}$ .

We consider a broken power law distribution of electrons generated via Fermi acceleration, written as

$$N(\gamma) d\gamma = K_o \gamma^{-p} \left(1 + \frac{\gamma}{\gamma_b}\right)^{-1} (\gamma_{min} \leq \gamma \leq \gamma_{max}) \quad (6)$$

where  $K_o$  is the normalization factor in electron density distribution,  $p$  is the electron power law distribution index which in our calculations is  $\sim 2$ .  $\gamma$  is the Lorentz factor,  $\gamma_{min}$  and  $\gamma_{max}$  are the minimum and maximum Lorentz factor respectively, and  $\gamma_b$  is the break Lorentz factor due to synchrotron cooling. The total power from synchrotron emission of a single electron is given by

$$P = \frac{4}{9} r_o^2 \beta^2 \gamma^2 B^2 \quad (7)$$

where  $r_o$  is the classical electron radius and  $\beta \equiv v/c$  (Rybicki & Lightman 1986). The corresponding synchrotron cooling time is

$$t_{cool} = \frac{\gamma m c^2}{P}. \quad (8)$$

The break Lorentz factor due to synchrotron cooling is obtained by equating the synchrotron cooling times scale and the dynamical timescale

$$t_d = \frac{R_o}{v_w} \quad (9)$$

where  $R_o$  is the standoff radius and  $v_w$  the wind velocity. The peak luminosity lasts for the pericenter crossing timescale with typical values  $\sim 1 \text{ yr}$ . The precise shape of the peak depends on the orbital parameters, the ambient gas distribution, and the wind mass loss rate. The characteristic timescale for the peak is the pericenter crossing time,  $\sim b/v$ .  $\gamma_{min}$  is set to one in our calculations.  $\gamma_{max}$  is obtained by equating the acceleration timescale,  $t_{acc} = \xi_{acc} R_L c / v_w^2$  (Blandford & Eichler 1987), to the dynamical or cooling timescale where  $\xi_{acc}$  is a dimensionless parameter on the order of unity. The Larmor radius is given by  $R_L = \gamma m_e c^2 / eB$  where  $m_e$  is the mass of the electron and  $e$  is the electron charge. We find that  $t_{acc} \sim 10^{-4} \text{ yr}$ , which is far shorter than the dynamic time. At radio frequencies the cooling time is a few orders of magnitude greater than the dynamical time and therefore synchrotron cooling is negligible. Thus, we assume that all the shocked electrons contribute to the observed synchrotron emission.

The synchrotron flux and power are computed using the radiative transfer equation (Rybicki & Lightman 1986) which leads to

$$I_\nu = \frac{j_\nu}{\alpha_\nu} (1 - e^{-\tau_\nu}) \quad (10)$$

where  $j_\nu$  is the emission coefficient,  $\alpha_\nu$  the absorption coefficient, and  $\tau_\nu$  the optical depth (see Wang & Loeb 2014 for further details).

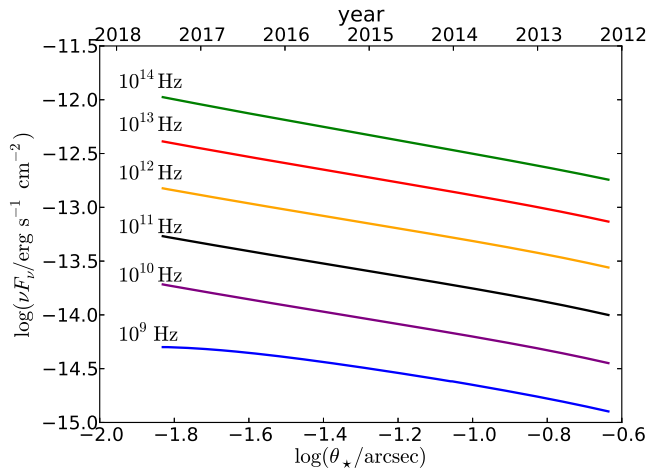


**Figure 2.** Synchrotron power (arcseconds) versus distance ( $\text{erg s}^{-1} \text{cm}^{-2}$ ) from Sgr A\* for star S2. We let  $\dot{M} = 10^{-6} M_{\odot} \text{yr}^{-1}$ . At a frequency of around 1 GHz, S2 is quite bright with a luminosity of  $\sim 10$  mJy. The synchrotron power will be greatest in 2017, when S2 is at periapease.

### 3 EMISSION AROUND SGR A\*

Figure 1 shows the expected synchrotron flux for a star orbiting Sgr A\*. For the left panel we kept the wind velocity constant at  $1000 \text{ km s}^{-1}$ . We extrapolated the particle density to have the value  $\sim 10^4 \text{ cm}^{-3}$  from Quataert (2004). The mass loss rate for hot massive stars is poorly constrained (for a review see Puls et al. 2008). Thus, we varied the mass loss rate between  $10^{-7} M_{\odot} \text{yr}^{-1}$  and  $10^{-5} M_{\odot} \text{yr}^{-1}$  which are acceptable values for hot massive stars such as the S-stars (Dupree 2015). Given that

$$F_{\nu} = \frac{\nu L_{\nu}}{4\pi d^2} \frac{1}{\nu} \quad (11)$$

where  $d = 8 \text{ kpc}$  we get a flux between  $\sim 10 - 1000$  mJy in the GHz range. Recently, Yusef-Zadeh et al. (2015) described radio observations of over 40 massive stars within  $30''$  of the GC. Their values for the flux are consistent with our results. Similar results were obtained when we kept the mass loss rate constant at  $10^{-6} M_{\odot} \text{yr}^{-1}$  and varied the wind velocity between  $1000 \text{ km s}^{-1}$  and  $4000 \text{ km s}^{-1}$  (see right panel of Figure 1).

In Figure 2 we plot the synchrotron power versus distance from Sgr A\* for S2. At periapease S2 has a speed of  $\sim 5500 \text{ km s}^{-1}$  while at apoapse the speed drops down to  $\sim 1300 \text{ km s}^{-1}$ . A higher speed leads to a stronger shock. However, even at apoapse it may very well be possible to observe the synchrotron emission from S2. At 10 GHz, S2 has a flux density of  $\sim 10$  mJy. Thus, S2 is an excellent target to observe. It is important to note that radio wavelength photons are scattered and the image size follows a  $\lambda^2$  dependence (e.g. Bower et al. 2006; Fish et al. 2014) of  $\sim 1 \text{ mas} (\lambda / \text{cm})^2$ . Therefore, in order to resolve S2 at the  $0.01''$  level, we need to observe at a frequency of 10 GHz or greater. Sgr A\* has been observed in the radio for decades. Kellermann et al. (1977) used very long baseline interferometry (VLBI) to observe Sgr A\* at 7.8 GHz, and they detected a nearby secondary transient source which has not been ex-

plained, and could in fact be S2 or another star. Furthermore, Herrnstein et al. (2004) monitored the flux density of Sgr A\* using the Very Large Array. Their results are consistent with our calculation. Macquart & Bower (2006) looked at the long-term variability of Sgr A\* and detected a flux of  $\sim 10^{31} \text{ erg s}^{-1}$  around the 1987 pericenter passage of S2. This indicates that the mass loss rate of S2 is  $\sim 10^{-6} M_{\odot} \text{yr}^{-1}$ . However, these data points are sparse and hence do not provide a tight constraint on the peak flux during the future pericenter passage.

While we expect the synchrotron emission to be detectable, the same is not necessarily true for the standoff radius. In Figure 3 we plot the standoff radius versus orbital radius. The standoff radius near the pericenter may not be resolvable, although at larger distances from Sgr A\* the likelihood for resolving the source increases. It is also worth noting that we calculated the thermal free-free emission around Sgr A\* and concluded that it is not detectable.

### 4 CONCLUSIONS AND FUTURE OBSERVATIONS

The innermost stars orbiting Sgr A\* (such as the S-stars) produce a bow shock. Although this shock will likely not be detectable via thermal emission, we have shown that stars such as S2 may be detectable via synchrotron emission. Figure 1 shows that the contrast of synchrotron flux relative to Sgr A\* is maximized around the 1.4 GHz band. However, due to scattering we will need to use a higher frequency, around 10 GHz, if we are to resolve our star. If a star such as S2 emits strong synchrotron emission, the combined signal from the star and Sgr A\* may exceed the quiescent radio emission from the black hole. As was the case with G2 (see next paragraph) it is not clear that any additional synchrotron emission will be observable. Arguably, it is best to resolve the synchrotron emission from any star orbiting Sgr A\*, such as S2. At apoapse S2 is  $\sim 0.23''$  from Sgr A\* while at periapease it is only  $\sim 0.015''$  away. Thus, to detect a star such as S2 requires both good sensitivity and resolution. VLBI can provide submilliarcsec observations of Sgr A\* (e.g. Lu et al. 2011) and thus the required precision. S2 is an ideal test case since the star will reach periapease in 2017 or early 2018.

Recently, gas cloud G2 was observed orbiting Sgr A\*, and was approximately 3100 Schwarzschild radii from the black hole at pericenter. It was predicted that the bow shock from this encounter would displace the quiescent radio emission of Sgr A\* by  $\sim 33 \text{ mas}$  (Narayan et al. 2012; Sadowski et al. 2013). However, observations across the spectrum showed no apparent variability during the periastron passage of G2 (Bower et al. 2015; Valencia-S et al. 2015). It is unclear why a bow shock was not detected. One possibility is that at the center of G2 is low-mass star with wind velocity  $\sim 100 \text{ km s}^{-1}$  (Crumley & Kumar 2013; Scoville & Burkert 2013). Synchrotron emission from such a small  $v_w$  would be extremely difficult to detect. Star S2 is massive, and thus the winds are likely an order of magnitude larger. If synchrotron emission is not detected for S2 it may be that our value for  $\epsilon_{nt}$  is too large. It may also be that the wind speeds from S2 are lower than expected, or that the number density around Sgr A\* is significantly less

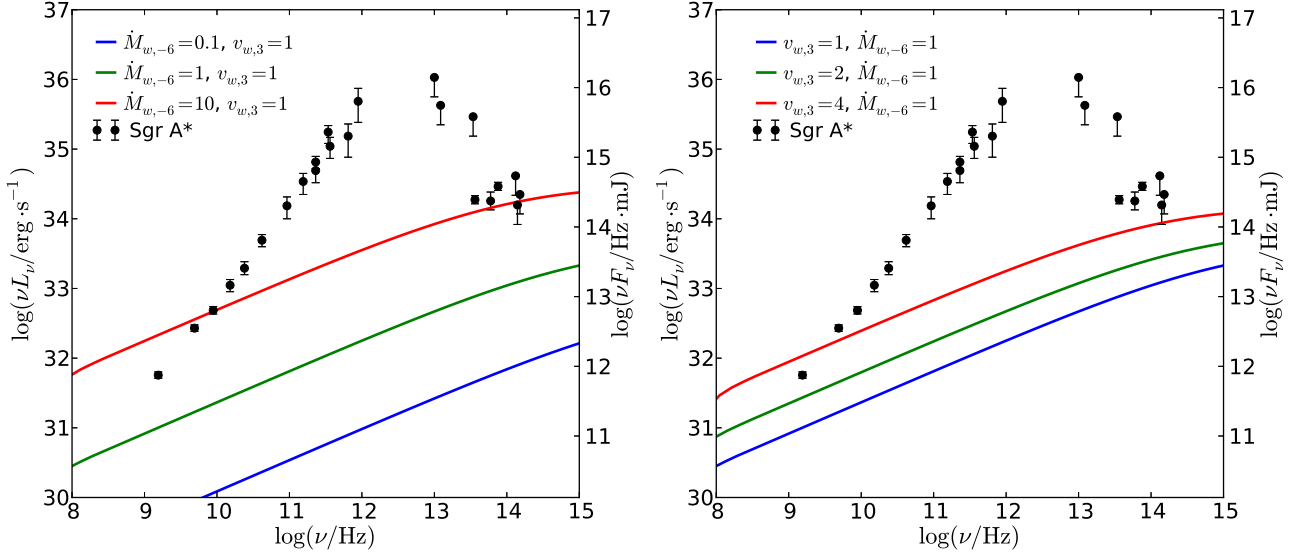


**Figure 1.** Non-thermal synchrotron power and flux compared with emission from Sgr A\* (data for Sgr A\* was obtained from Yuan & Narayan 2014). The left panel shows the dependence of the synchrotron emission on wind mass loss rate. The star’s velocity and wind velocity are both fixed at 1000 km s<sup>-1</sup>. Mass loss,  $\dot{M}$ , was computed with values of  $10^{-7}M_{\odot}$  yr<sup>-1</sup> (blue line),  $10^{-6}M_{\odot}$  yr<sup>-1</sup> (green line), and  $10^{-5}M_{\odot}$  yr<sup>-1</sup> (red line). In the right panel we kept the mass loss constant at  $10^{-6}M_{\odot}$  yr<sup>-1</sup> and used wind velocities of 1000 km s<sup>-1</sup> (blue line), 2000 km s<sup>-1</sup> (green line), and 4000 s<sup>-1</sup> (red line).

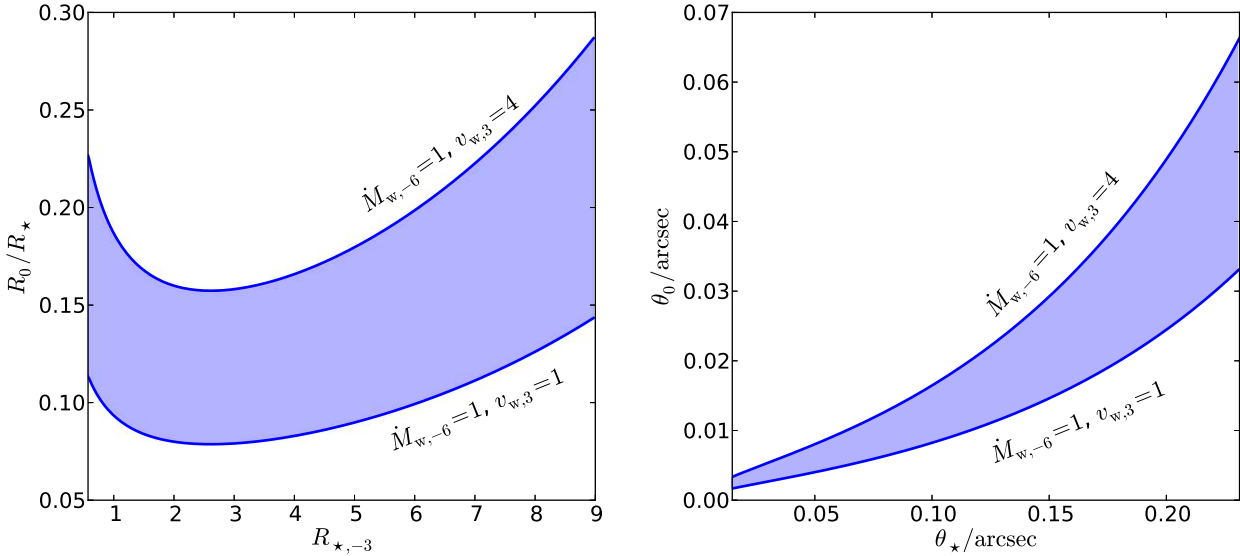


**Figure 3.** Left: The standoff radius for S2 ( $R_o$ ) versus the orbital radius ( $R_*$  in units of  $10^{-3}$  pc). We see that the value is always less than unity, as expected. Right: angular diameter of the standoff radius ( $\theta_o$ ) versus the angular diameter of the orbital radius ( $\theta_*$ ). Around pericenter it may be difficult to resolve the finite size of the standoff radius. However, S2 should still be detectable via synchrotron emission.

than what is predicted. Arguably, the most likely reason why synchrotron emission from S2 may not be detected is simply that the shock is not as strong as assumed. Our results are valid so long as the shock is strong, but the emission could be much fainter if the strength of the shock is lessened. Since the shock will be strongest when S2 passes periape, this will be the ideal time to monitor the star for synchrotron emis-

sion. Even a null detection will help place constraints on the environment around Sgr A\* (Giannios & Sironi 2013).

In addition to radio observations at around the 10 GHz band, Figure 1 shows that at infrared wavelengths, in particular around  $10^{14}$  Hz, Sgr A\* is approximately the same luminosity as a close-by star such as S2. However, S2 itself emits in the infrared, therefore we will not be able to distinguish between the non-thermal and thermal emission. We

will need to compare the measured flux with that of the S2. An instrument with enough sensitivity, such as the James Webb Space Telescope (JWST), should be able to detect the synchrotron emission in the infrared. JWST is scheduled to launch in October of 2018. While S2 will have passed pericenter, if our predictions are correct the synchrotron emission should still be detectable. Furthermore, it may be possible to measure the increase in total infrared emission from S2 between apocenter and pericenter owing to the increased synchrotron emission. While S2 is the litmus test for detecting stars at the Galactic Centre via synchrotron emission, we hope that ultimately we can use this technique to detect and monitor stars that have thus far not been observable.

### ACKNOWLEDGMENTS

We thank Michael D. Johnson, Atish Kamble, Robert Kimberk, Mark Reid, Lorenzo Sironi, and Ryo Yamazaki for helpful comments. This work was supported in part by Harvard University and NSF grant AST-1312034.

### REFERENCES

Blandford R., Eichler D., 1987, *PhR*, 154, 1  
 Bower G., S. M., J. D., Gurwell M., Moran J., Brunthaler A., Falcke H., Fragile P., Maitra D., Marrone D., Peck A., Rushton A., Wright M., 2015, *ApJ*, 802, 69  
 Bower G., W.M. G., H. F., Backer D., Lithwick Y., 2006, *ApJL*, 648, L127  
 Brown W., Anderson J., Gnedin O., Bond H., W.R. Geller M., Kenyon S., 2015, *ApJ*, 804, 49  
 Brown W., Geller M., Kenyon S., 2014, *ApJ*, 787, 89  
 Brown W., Geller M., Kenyon S., Kurtz M., 2005, *ApJL*, 622, L33  
 Chen X., Amaro-Seoane P., 2014, *ApJL*, 786, L14  
 Crumley P., Kumar P., 2013, *MNRAS*, 436, 1955  
 Dupree A. K., 2015, private communication  
 Fish V., Johnson M., Lu R., Doeleman S., et al. 2014, *ApJ*, 795, 134  
 Genzel R., Eisenhauer F., Gillessen S., 2010, *Rev. Mod. Phys.*, 82, 3121  
 Ghez A., Duchêne G., Matthews K., Hornstein S., Tanner A., Larkin J., Morris M., Becklin E., Salim S., Kremenek T., Thompson D., Soifer B., Neugebauer G., McLean I., 2003, *ApJL*, 586, L127  
 Ghez A., Salim S., Hornstein S., Tanner A., Lu J., Morris M., Becklin E., Duchêne G., 2005, *ApJ*, 620, 744  
 Ghez A., Salim S., Weinberg N., Lu J., Do T., Dunn J., Matthews K., Morris M. R., Yelda S., Becklin E., Kremenek T., Milosavljevic M., Naiman J., 2008, *ApJ*, 689, 1044  
 Giannios D., Sironi L., 2013, *MNRAS*, 433, L25  
 Gillessen S., Eisenhauer F., Fritz T., Bartko H., Dodds-Eden K., Pfuhl O., Ott T., Genzel R., 2009, *ApJL*, 707, L114  
 Gillessen S., Eisenhauer F., Trippe S., Alexander T., Genzel R., Martins F., Ott T., 2009, *ApJL*, 692, 1075  
 Ginsburg I., Brown W., Wegner G., 2013, arXiv:1302.1899  
 Ginsburg I., Loeb A., 2006, *MNRAS*, 368, 221  
 Ginsburg I., Loeb A., 2007, *MNRAS*, 376, 492

Ginsburg I., Loeb A., Wegner G., 2012, *MNRAS*, 423, 948  
 Griv E., 2010, *ApJ*, 709, 597  
 Guo X., Sironi L., Narayan R., 2014, *ApJ*, 794, 153  
 Herrnstein R., Zhao J.-H., Bower G., Goss W., 2004, *AJ*, 127, 3399  
 Hills J., 1988, *Nature*, 331, 687  
 Kellermann K., Shaffer D., Clark B., Geldzahler B., 1977, *ApJL*, 214, L61  
 Löckmann U., Baumgardt H., Kroupa P., 2008, *ApJ*, 683, 151  
 Lu R.-S., Krichbaum T., Eckart A., König S., Kunneriath D., Witzel G., Witzel A., Zensus J., 2011, *A&A*, 525, 76  
 Macquart J.-P., Bower G., 2006, *ApJL*, 641, 302  
 Mapelli M., Gualandris A., 2015, arXiv:1505.05473v1  
 Martins F., Gillessen S., Eisenhauer F., Genzel R., Ott T., Trippe S., 2008, *ApJ*, 672, L119  
 Meyer L., Ghez A., Schödel R., Yelda S., Boehle A., Lu J., Do T., Morris M., Becklin E., Matthews K., 2012, *Science*, 338, 84  
 Narayan R., Özel F., Sironi L., 2012, *ApJL*, 757, L20  
 Palladino L., Schlesinger K., Holley-Beckelmann K., Prieto C., Beers T., Lee Y., Schneider D., 2014, *ApJ*, 780, 7  
 Puls J., Vink J., Najarro F., 2008, *A&ARv*, 16, 209  
 Quataert E., 2004, *ApJ*, 613, 322  
 Rybicki G., Lightman A., 1986, *Radiative Processes in Astrophysics*. Wiley, New York  
 Sadowski A., Sironi L., Abarca D., Guo X., Özel F., 2013, *MNRAS*, 432, 478  
 Schödel R., Merritt D., Eckart A., 2009, *A&A*, 502, 91  
 Schödel R., Najarro F., Muzic K., Eckart A., 2010, *A&A*, 511, A18  
 Schödel R., Ott T., Genzel R., Eckart A., Mouawad N., Alexander T., 2003, *ApJ*, 596, 1015  
 Scoville N., Burkert A., 2013, *ApJ*, 768, 108  
 Valencia-S M., Eckart A., Zajaček M., et al. 2015, *ApJ*, 800, 125  
 Völk H., Berezhko E., Ksenofontov L., 2005, *A&A*, 433, 229  
 Wang X., Loeb A., 2014, *MNRAS*, 441, 809  
 Yuan F., Narayan R., 2014, *ARAA*, 52, 529  
 Yusef-Zadeh F., Bushouse H., Schödel R., Wardle M., Cotton W., Roberts D., Noguera-Lara F., Gallego-Cano E., 2015, arXiv:1506.07182v1  
 Zhang F., Youjun L., Qingjuan Y., 2013, *ApJ*, 768, 153  
 Zhang Y., Smith M., Carlin J., 2015, arXiv:1501.07824v1  
 Zhong J., Chen L., Chao L., De Grijs R., Hou J., Shen S., Shao Z., Li J., Lou A., Shi J., Zhang H., Yang M., Deng L., Jin G., Zhang Y., Hou Y., Zhang Z., 2014, *ApJL*, 789, L2

This paper has been typeset from a  $\text{\TeX}$ / $\text{\LaTeX}$  file prepared by the author.